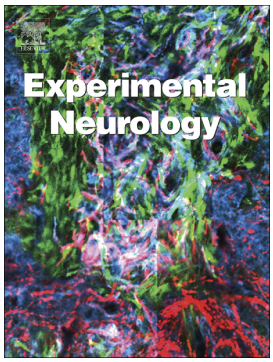

Neural stem cell-derived exosomes-loaded adhesive hydrogel controlled-release promotes cerebral angiogenesis and neurological function in ischemic stroke

Chenyang Gu, Yajing Li, Jiale Liu, Sitian Liu, Jun Long, Qiankun Zhang, Wenjie Duan, Tingle Feng, Jiajun Huang, Yunhui Qiu, Waqas Ahmed, Hengsen Cai, Yong Hu, Yaobin Wu, Lukui Chen

PII: S0014-4886(23)00232-7

DOI: https://doi.org/10.1016/j.expneurol.2023.114547

Reference: YEXNR 114547

To appear in: *Experimental Neurology*

Received date: 21 April 2023

Revised date: 31 August 2023

Accepted date: 21 September 2023

Please cite this article as: C. Gu, Y. Li, J. Liu, et al., Neural stem cell-derived exosomes-loaded adhesive hydrogel controlled-release promotes cerebral angiogenesis and neurological function in ischemic stroke, *Experimental Neurology* (2023), https://doi.org/10.1016/j.expneurol.2023.114547

Neural Stem Cell-Derived Exosomes-Loaded Adhesive Hydrogel Controlled-Release Promotes Cerebral Angiogenesis and Neurological Function in Ischemic Stroke

Chenyang Gu[1,2,†], Yajing Li[3,†], Jiale Liu[1,†], Sitian Liu[4,†], Jun Long[1], Qiankun Zhang[1], Wenjie Duan[1], Tingle Feng[1], Jiajun Huang[1], Yunhui Qiu[5], Waqas Ahmed[3], Hengsen Cai[6], Yong Hu[7], Yaobin Wu[4,#] and Lukui Chen[1,#]

[1]Department of Neurosurgery, Neuroscience Centre, Integrated Hospital of Traditional Chinese Medicine, Southern Medical University, Guangzhou 510310, P.R. China.

[2]Department of Neurology, Affiliated Zhongda Hospital, School of Medicine, Southeast University, Nanjing 210009, P.R. China.

[3]The tenth Affiliated Hospital of Southern Medical University (Dongguan People's Hospital), Dongguan 523059, P.R. China.

[4]Guangdong Engineering Research Centre for Translation of Medical 3D Printing Application, Guangdong Provincial Key Laboratory of Medical Biomechanics, Department of Human Anatomy, School of Basic Medical Sciences, Southern Medical University, Guangzhou 510515, P.R. China.

[5]Department of Pathology, Integrated Hospital of Traditional Chinese Medicine, Southern Medical University, Guangzhou 510310, P.R. China.

[6]Department of Neurosurgery, The Second People's Hospital of Pingnan, Pingnan 537300, P.R. China.

[7]Department of Orthopaedics and Traumatology, The University of Hong Kong, Hongkong 999077, P.R. China.

† These authors have contributed equally to this work and share first authorship.

Correspondence: Prof. Lukui Chen, neuro_clk@hotmail.com, Tel: +86-13922791031, 13 Shiliugang Rd, Haizhu District, Guangzhou, China; Prof. Yaobin Wu, wuyaobin2018@smu.edu.cn, Tel: +86-13068803827, 1023-1063 Shatai Rd S, Baiyun District, Guangzhou, China.

Abstract

Objective: Ischemic stroke has become one of the leading diseases for international death, which brings burden to the economy and society. Exosomes (Exos) derived following neural stem cells (NSCs) stimulation promote neurogenesis and migration of NSCs. However, Exos themselves are easily to be removed in vivo. Our study is to investigate whether adhesive hyaluronic acid (HAD) hydrogel loading NSCs-derived-Exo (HAD-Exo) would promote the recovery of ischemic stroke. **Methods:** A mouse model of middle cerebral artery occlusion (MCAO) was established. PBS, Exo, HAD, and HAD-Exo groups were independently stereotactically injected in mice, respectively. The modified neurological severity score scale and behavior tests were used to evaluate neurological improvement. Neuroimagings were used to observe the improvement of cerebral infarct volume and vessels. Immunofluorescence staining was used to verify the expression of vascular and cell proliferation-related proteins. **Results:** The structural and mechanical property of HAD and HAD-Exo were detected. Behavioral results showed that HAD-Exo significantly improved neurological functions, especially motor function. Neuroimagings showed that HAD-Exo significantly promoted infarct volume and angiogenesis. Immunofluorescence staining showed that HAD-Exo significantly promoted the cerebral angiogenesis and anti-inflammation. **Conclusion:** NSCs derived

exosomes-loaded adhesive HAD hydrogel controlled-release could promote cerebral angiogenesis and neurological function for ischemic stroke.

Keywords: neural stem cell; exosome; adhesive hydrogel; controlled-release; ischemic stroke; angiogenesis.

Introduction

Stroke is still a major disease that seriously endangers human life and health, with high rates of disability and fatality (Tsao et al., 2023). There are approximately 80 million stroke patients globally, with over 14 million in China (Sharma et al., 2022). Most survivors have varying degrees of disability, which seriously affects their physical and mental quality of life and that of their families, and is economically detrimental (Lin et al., 2019; Sharma et al., 2022). From the aspect of pathogenesis, 85% of stroke cases are ischemic stroke (IS) (Tsao et al., 2023). IS results from blockage of intracranial blood vessels, leading to apoptosis or necrosis of cells of the brain. Neurovascular changes and brain damage can result. Secondary cellular damage is coordinately mediated by multiple pathophysiological mechanisms after IS, such as oxidative stress (Orellana-Urzúa et al., 2020), inflammation (Zhang, 2018), energy depletion (Mendelson and Prabhakaran, 2021), vascular dysfunction (Mendelson and Prabhakaran, 2021), excitotoxicity, apoptosis, and autophagy (Coscia et al., 2019). Treatment of IS mainly involves mechanical thrombectomy or intravenous thrombolysis with recombinant tissue-type plasminogen activator to restore blood flow. The narrow time window limits the effectiveness and safety of treatment (Adams et al., 2007). Developing other more effective treatments is important. The Middle Cerebral Artery Occlusion (MCAO) mice model is the most common animal model for IS studies.

Stem cells (SCs) that are present in human embryos, umbilical cord blood, and adults can self-renew in an undifferentiated state, while retaining the ability to differentiate into other specific cell types (Obernier and Alvarez-Buylla, 2019). Stimulation with external factors and/or components of damaged host cells from the tissue microenvironment trigger the proliferation, migration, and differentiation of SCs (Rong et al., 2019). Neural SCs (NSCs) are one of the most important SC types in the nervous system. NSCs can differentiate to specific neurons in culture (Llorens-Bobadilla et al., 2022). NSCs are homologous with neurons and other cells in the brain, which can avoid heterogeneous immune response and tumorigenicity during treatment (Chen et al., 2022; Lyu et al., 2021).

Exosomes (Exos) derived from eukaryotic cells, are extracellular vesicles that are much smaller than microvesicles, red blood cells, and apoptotic bodies, with diameters of 30–200 nm (Contreras et al., 2022). Exos either budded through the plasma membrane or are directly released from cells. The variety of contents of Exos include RNA, proteins, lipids, cytokines, and chemokines, among others (Johnstone et al., 1987). Functionally, Exos mediate cell proliferation, migration, division, and apoptosis, are involved in immune regulation, maintain homeostasis, and are involved in disease development (Genet and Hirschi, 2021). In addition, Exos participate in coagulation, waste management, and intercellular signalling transduction (Reed and Escayg, 2021). In our previous studies, we found that the exosomes contained the active components of cells, could cross the BBB freely, load drugs (Zhu et al., 2023), promote neurogenesis and anti-inflammation (Long et al., 2023; Zhang et al., 2020), and could be labelled for targeted therapy etc. (Zhang et al., 2019)

Traditional hydrogels have been widely used in tissues and organs. These hydrogels have high water contents, are pliable, and display a tissue-like three-dimensional (3D) environment (Gu et al., 2021; Shao et al., 2019). First-generation hydrogels did not interact with tissues when applied *in vivo* and were not universal in their application for focal lesions (Cook et al., 2017; Darling et al., 2020). These limitations led to the modified design and preparation of an injectable hydrogel with superior tissue retention properties that could adhere to tissue surface to release Exos in a controlled manner (Ju et al., 2014). The modified hyaluronic acid (HAD) hydrogel modified by catechol (Wu et al., 2021), which could encapsulate NSC-derived Exos, and maintain Exo activity. The HAD hydrogel could mimic the 3D microenvironment of tissues to induce endogenous cell adhesion and proliferation, and enhance angiogenesis in the region of ischemia.

In the present study, we used a novel injectable adhesive hydrogel. The photocurable catechol-grafted HAD hydrogel maintained adhesion and sustained release of Exos. The HAD precursor facilitated adhesion on tissue surface, while the nonadherent region of the hydrogel formed after photocrosslinking displayed anti-adhesive activity to prevent scar adhesion and mechanical damage of wounds. We envisage the application of a combined therapy of Exos and HAD hydrogel to effectively improve neurological function, angiogenesis, and inflammation of the whole brain following IS.

Experimental

Animals & Grouping

All animals were treated in accordance with Southeast University, and the animal protocols were approved by the Ethics Committee of Southeast University (ethical number: 20210405006, approval date: 2021.04.05). 62 C57BL/6J adult male mice

(weighing 20-25 g and 6-8 weeks old) and 6 C57BL/6J adult female mice (pregnant 15-day), provided by the Animal Experiment Centre of Southeast University. All grouping, operations and evaluations were performed by three professionals who were blinded to the experimental design with stratified randomization to minimize potential confounders. All involved experimental animals were anesthetized by intraperitoneal injection (IPI) of 2% amobarbital based on 45 mg/kg body weight. (Gu et al., 2022; Xu et al., 2010)

After the operation, based on the stratified randomization, 62 mice (weighing 20-25 g and 6-8 weeks old) were involved in grouping, in which 6 mice in Sham group (mice were given stereotactic injection of 2μL PBS, the coordinates: Bregma -0.5 to 0.02 mm; lateral: left 1.8 to 2.2 mm; depth: -4 to -1 mm), and 56 mice in MCAO operation. 24 h after surgery, 13 mice with modified Neurological Severity Score (mNSS) of 13-18 died (20-23% mortality), which were due to MCAO operation. 7 mice with mNSS of 0 were withdrawn from the experiment.

There were 12 mice, 3 mice of each group (PBS, Exo, HAD, Had-Exo groups) for "In vivo imaging & tracing of PKH26-Exo" experiments.

The 30 mice left were divided into 4 groups: PBS group, in which the MCAO model mice were given stereotactic injection (The coordinates: Bregma -0.5 to -0.35 mm; lateral: left 1.8 to 2.2 mm; depth: -4 to -1 mm) of PBS 2 μL; Exo group, in which the MCAO model mice were given a stereotactic injection of Exos 2 μL, approximately 10^{10} particles; HAD group, in which the MCAO model mice were given a stereotactic injection of HAD precursor 2 μL; HAD-Exo group, in which the MCAO model mice were given a stereotactic injection of HAD-Exo 2 μL, approximately 10^{10} particles. The stereotactic injections for treatments/PBS were administrated immediately following MCAO operation.

Culturing of NSCs and isolation of Exos

NSCs were obtained from the hippocampus of foetal mouse brain (extracted from 6 pregnant mice in total) and cultured in growth medium with F12/DMEM (Gibco, Grand Island, NY, USA), 2% B27 (Gibco, Grand Island, NY, USA), bFGF 20 ng/ml (Novoprotein Scientific Inc., Suzhou, China), and EGF 20 ng/ml (Sino Biological Inc., Beijing, China) (B27/F12 medium).

Mice on day 15-16 of pregnancy were anesthetized by IPI of amobarbital, hair was shaving on the abdomen skin, disinfected with iodophor cotton balls 3 times, deionized with 75% ethanol. The uterus was removed by laparotomy under aseptic conditions, and then the female mice were sacrificed. E15-16 embryos were isolated from the uterus, and the hippocampal tissue of the embryonic brain was isolated under a stereomicroscope. 10 mL of B27/F12 medium was added, and the hippocampal tissue was mechanically blowing to prepare cell suspension. Undispersed tissue pieces were removed by 400-mesh filter, and the filtered cell suspension was cultured in B27/F12 medium at 37 °C and 5% CO2 for subsequent experiments.

The growth medium of NSCs was collected and centrifuged at 300 ×g for 10 min to remove cells, followed by centrifugation at 2,000 ×g for 10 min to remove dead cells at 4 °C. The supernatant collected was centrifugation at 10,000 ×g for 30 min to remove cell debris, followed by centrifugation at 150,000 ×g for 70 min to obtain exosomes at 4 °C using Optima XPN-100 Ultracentrifuge (Beckman Coulter, Asphalt, CA, USA). The sediment was diluted in Phosphate Buffer Saline (PBS), stored at −80 °C or used immediately for experiments.

Identification of NSCs

NSCs were planted on poly-lysine-coated glass slides for cell adhesion, which were fixed with paraformaldehyde (PFA, 4%, w/v, pH 7.4), permeated with 0.3% Triton X-100, and blocked with goat serum. The NSC spheres were labelled with the NSCs markers Nestin antibody at 4 ℃ overnight, and then treated with fluorescent second at room temperature for 2 h. The nuclei were stained with 4', 6-diamidino-2-phenylindole (DAPI), and the plates were sealed and fixed, and detected by immunofluorescence (IF) staining with fluorescence microscopy.

Transmission electron microscope (TEM)

Exosomes isolated immediately were fixed with 2.5% glutaraldehyde at 4 °C overnight. After washing, vesicles were loaded onto formvarcarbon-coated grids, negatively stained with aqueous phosphotungstic acid for 60 s and imaged with a TEM at 80 kV (HT-7700 TEM, Hitachi).

Nanoparticle tracing analysis (NTA)

NTA was performed by Zetaview (Particle Metrix) to characterize the particles per ml of exosomes. Exosomes collected from supernatant were diluted in 1 ml of PBS as needed and evaluated. A particle size distribution plot was created with estimated particle diameter (nm) on the X-axis and concentration (particles/mL) on the Y-axis. Besides, a particle size distribution plot based on intensity was generated with estimated particle diameter (nm) on the X-axis and intensity (a. u.) on the Y-axis.

Western blotting (WB)

WB was used to evaluate exosome surface markers using specific antibodies: anti-tumour susceptibility 101 (TSG101, rabbit Polyclonal, DF8427, Affinity, Jiangsu, China), anti-CD81 (rabbit monoclonal, Zenbio, China), CD63 (rabbit monoclonal, Affinity, Jiangsu, China) and calnexin (rabbit monoclonal, Zenbio, China).

Preparation of adhesive hydrogel (HAD)

The HAD precursor was fabricated by grafting 3,4-dihydroxyphenylalanine (DA) and 2-aminoethyl methacrylate (AEMA) on hyaluronic acid (HA) chain. DA and AEMA served as the wet adhesive and photocurable groups, respectively. For HAD polymer synthesis, HA (1 g) was dissolved in 100 mL of deionized water at a concentration of 1%w/v. 1-(3-Dimethylaminopropyl)-3-ethylcarbodiimide hydrochloride (EDC, 4 mmol), N-Hydroxy succinimide (NHS, 4 mmol), and AEMA were slowly added to the solution and stirred for 30~40 mins. Subsequently, dopamine hydrochloride was added to the mixture for 24 h. All solutions were kept under nitrogen protection and stored in darkness at room temperature to prevent oxidation. The pH value was monitored and adjusted between 5~6 with 0.1 N hydrochloric acid and sodium hydroxide. After the reaction, the unreacted monomers were eliminated by dialysis (MWCO = 8000~12000 Da) under acidic conditions for 72 h and then lyophilized. The lyophilized extract(s) foam was stored in a closed container and kept from light till used. The mass ratios of HA:AEMA:DA was 1:3:3, and these polymers were named as H-3A-3D (HAD). The HAD hydrogel was formed at 365 nm under UV crosslinking for only 3–5 s using lithium phenyl-2,4,6-trimethylbenzoylphosphinate as the photoinitiator (**Fig. 2A-C**). The HAD-Exo complex is consisted of 30 mg HAD precursor + 1 ml 5×10^{12} particles/ml Exo/PBS supernatant. Each mouse in the HAD-Exo group was injected stereotactically with 2 μL to ensure that the number of exosomes were maintained at 10^{10} particles/mouse.

Scanning electron microscope

After freezing drying, the hydrogel samples were sputter-coated with a thin layer of gold under a vacuum chamber. The cross-section and surface morphologies of the samples were observed by a field emission scanning electron microscope (N7000, Hitachi).

Adhesive test

The viscosity of the HAD precursor solution decreased exponentially as the shear rate was increased at 37 °C. This indicated that HAD precursors solution had good shear thinning behaviour and could be conveniently administered as an injection [16]. After the hydrogel precursors were attached to the brain and the adhesive, the adhesive was lifted after UV curing to observe whether the brain fell off. The adhesion was observed under running water.

Swelling ratio (SR) & rheological property

The SR behaviour of the hydrogel was determined as follows. The lyophilized hydrogel cylindrical shape samples were put into 20 mL of PBS (pH 7.4) in sealed vials at 37 °C. Hydrogel samples (5 samples for each group) were taken out from PBS at pre-set time intervals, and superficial water on the swollen gel. Immediately after removal of water using filter paper, the net weight of hydrogel was recorded at pre-set time intervals. The SR was calculated by the following equation: $SR= (W_t - W_0)/W_0\times100\%$, where W_0 and W_t represented the 5 initial weight of the wet hydrogel and the weight after swelling pre-set time, respectively. The test was repeated three times.

Rheological properties of HAD hydrogel with time frequency-sweep (0.1–10 Hz, strain of 1%) test using Anton Paar Instruments MCR102e stress controlled rheometer fitted with a Peltier stage set to 37 °C. Dynamic oscillatory strain amplitude sweep measurements were conducted at a frequency of 10 rad/s. Dynamic oscillatory frequency sweep measurements were conducted at a 2% strain amplitude. All measurements were performed using a 20 mm 4° cone geometry.

3D imaging of laser scanning confocal microscopy

Exosome encapsulated hydrogel were photocured and their 3D images were taken under confocal microscopy.

Transwell test

Boyden chamber assays were performed using 24-well transwell inserts (Corning, NY, USA) with 8 μm poresized filters and 24-well culture plates as described previously. hydrogel was cured by ultraviolet light and plated into the upper chamber. 1000 μL Hyaluronidase medium with PBS was added to the lower chamber. After incubation for 1st, 3rd, 5th, 7th, 14th, 21st and 28th day, The OD value of protein in the 1ml liquid of the chamber was measured by BCA method each time and replaced with a new 1ml PBS of dissolved hyaluronidase.

MCAO Modelling

Suture method: All mice were anesthetized by IPI of 2% amobarbital based on 45 mg/kg body weight. After the righting reflex disappeared, the neck midline was incised, the muscle was bluntly separated, the slightly pulsating common carotid artery (CCA) was seen, and the accompanying vagus nerve was separated with glass needle; the external carotid artery (ECA), internal carotid artery (ICA), and CCA crossed a "Y" shape. The CCA is ligated, and the ICA is clamped; the ECA approach leads to the monofilament, when the black mark of the monofilament (head diameter: 0.2 ± 0.02 mm, body diameter: 0.14 mm, length: 30 mm; Jialing Corporation, Guangzhou, China) reaches the Y-shaped bifurcation. After the monofilament is left for 60 minutes, the wound will be sutured.

In vivo imaging & tracing of PKH26-Exo

The PKH26-stained exosomes (PKH26-Exo) were premixed with adhesive hydrogel (HAD-PKH26-Exo). Using a microinjection needle, the PBS, PKH26-Exo, HAD and HAD-PKH26-Exo were injected stereotactically into the ischemic penumbra area immediately after the operation of the MACO model, respectively. The hydrogel distribution was observed on pre-treatment (PT, 24h following MCAO) and day 7th, 14th, 21st and 28th after injection with small animal imager (IVIS Lumina XRMS In Vivo Imaging System, Perkin Elmer, USA).

Behavioural Tests

mNSS

The mNSS evaluates the mice comprehensively from all aspects of movement posture, response to stimuli and coordination and reflexes during body position transformation. For normal mice, the score was 0, the mNSS between 1 and 6 was mild injury, between 7 and 12 was moderate injury, and between 13 and 18 was severe injury at agonal stage. The data were collected at the timepoint of PT, 7th, 14th, 21th and 28th day after MCAO surgery.

Grip of front paws

Let the forelimb of the mice grasp the metal triangle rod of muscle strength detector, and slowly drag the tail of the mice backward. When the forelimb of the mice released, the highest value was recorded as the maximum grip. Each mouse was measured 5 times, and the average value was calculated for statistical analysis. The data were collected at the timepoint of Pre-OP, PT, 7th, 14th, 21th and 28th day after MCAO surgery.

Rotarod system

The mice were placed on a rotating stick and turned at a constant speed of 10 rpm/min. The speed was gradually increased to 40 rpm/min (accelerated speed: 5 rpm/min), and the Retention time of each mouse on the rod was measured. Due to the impaired motor function and physically tired, the mice finally occurred to falling off the stick with speed increase. The Retention time and Rotate speed of drop was also collected at the timepoint of Pre-OP, PT, 7th, 14th, 21th and 28th day after MCAO surgery.

CatWalk gait analysis

The mice of groups were allowed to enter the CatWalk runway smoothly, and the mice were allowed to traverse the runway spontaneously and without stopping under any stimulus. The test mice passed the runway 3 times without interruption and at a roughly uniform speed within 5s. The gait parameters were collected in PT (24h after MCAO) and 28th day treatment after MCAO surgery.

Laser speckle imaging system (LSIS)

The blood perfusion volume and vessel diameter were measured by LSIS. The skin was cut through the midsagittal line of the cranial apex and the serosal membrane on the skull surface was peeled off. Two drops of bupivacaine hydrochloride were added for local analgesia, and then the skull was polished with a skull drill until the angiography was clear. Adjust the focal length, false colour threshold and magnification parameters. Optical imaging was performed again at PT, 7th, 14th, 28th day after MCAO and treatment. The cerebral blood flow perfusion and infarct volume were extracted from the image information offline, and the percentage values of cerebral ischemia were calculated according to the basic values. ImageJ was used to quantify the infarct volume and ratio of the ischemic area. Briefly, the infarct volume in LSIS analysis was calculated by the ratio of infarct area without blood flow to the whole brain area in top view, then the statistical analysis was administrated.

MRI

All mice were anesthetized by IPI of 1% pentobarbital based on 45 mg/kg body weight. The heart rate of mice was monitored to judge dynamically the physical condition. Conventional Magnetic Resonance Imaging (MRI; PharmaScan70/16 US, Bruker, USA) in Southern Medical University was utilized to dynamically evaluate the infarct volume at the timepoint of PT, 7th, 14th and 28th day after MCAO surgery *in vivo*. The sequence protocol was executed with the following parameters: T2-weighted; 256×256 matrix; slice thickness, 1 mm; intersection gap, 1 mm; echo time/repetition time: 27/3000 ms; rapid acquisition with relaxation enhancement factor, 16; flip angle, 90 degrees. Image J was used to quantify the infarct volume and ratio of the ischemic area. Specifically, the infarct volume in MRI analysis was calculated by the ratio of infarct area to the whole brain area in different Bregma levels, then the statistical analysis were administrated.

Nissl staining

The animals received "Perfusion death" after 28 days treatment aim at Immunohistochemistry analysis. The fresh tissue was fixed in 10% neutral formalin solution for 48h and then dehydrated and embedded. The sections were 6-8 μm thick and were conventionally dewaxed to water. The slices were put into Toluidine blue Stain, and the staining cylinder was placed in an incubator at 50-60 °C and infected for 25-50min. Rinse with 70% ethanol after slightly rinsed with distilled water; 95% ethanol differentiates rapidly. Rapid dehydration of anhydrous ethanol; Xylene transparent, neutral gum seal; They were then photographed under a microscope.

IF staining

NSCs were fixed with precooled paraformaldehyde (4%, w/v) for 20 min, then permeabilized with 0.3% Triton X-100 for 15 min, blocked with 10% normal goat serum for 1.5h, and finally incubated overnight at 4 °C with the following primary antibodies: anti-nestin (1:250, mouse IgG; CST, USA), anti-BrdU (1:300, mouse IgG; CST, USA), anti-vWF (1:250, rabbit IgG; Abcam, USA), anti-CD31 (1:250, rabbit IgG; Proteintech, Wuhan, China), anti-SMA-α (1:250, rabbit IgG; Proteintech, Wuhan, China), anti-TNF-α (1:250, rabbit IgG; Affinity, USA), anti-IL-1 (1:250, rabbit IgG; Affinity, USA). The following day, the cells were treated with secondary antibody at room temperature for 2 h and the nuclei were counter-stained for 1 min with DAPI. Immunoreactivity was visualized using a fluorescence microscope (IX53, Olympus, Japan). Image J was used to quantify the fluorescence intensity of the ischemic area.

TUNEL staining

The prepared frozen sections were washed with PBS for 3 times. The samples were incubated in proteinase K working solution at 37 ℃ for 30min. Then wash with PBS for 3 times; Treatment with H_2O_2 at room temperature for 10min; After washing with PBS for 3 times, the TdT enzyme reaction solution was used to incubate at 37 ℃ for 60min in the dark. After washing with PBS for 3 times, the treatment was carried out in Streptavidin-HRP solution at 37 ℃ for 30min and protected from light. Wash with PBS for 3 times and use DAB for colour development; Then wash with PBS 3 times; Finally, the film was re-dyed with haematoxylin after processing and shot in the open field. Image J was used to quantify the fluorescence intensity of the ischemic area.

Enzyme-linked immunosorbent assay (ELISA)

Animals were administrated to collect blood through tail amputation for ELISA. Then the blood was collected in tube without anticoagulant, and stood at RT for 60 min to wait for the blood clotting; to rupture the blood clot, equilibrate overnight at 4, and centrifuge at 1000 rpm for 10 min, and the supernatant was the required serum. The production of TNF-α, IL-1 (Elabscience Biotechnology Co., Ltd, China) was measured using ELISA kits according to the manufacturer's instructions. Briefly, based on the standard and blank wells, the same volume of samples was added to the sample wells, and 6 parallel wells were set up for each experiment. Cover the microtiter plate with film and incubate at 37 ℃ for 30 min. Then the biotin antibody working solution was add in each well, incubating for 1 h at 37 ℃. The enzyme conjugate working solution was added, incubating for 30 min at 37 ° C. The substrate solution was added, incubating at 37 ° C for 15 min. Finally, stop solution was added to terminate the reaction, and the OD value was measured in a microplate reader at a wavelength of 450 nm.

Statistical analysis

Data analyses were performed using the software SPSS 26.0 and GraphPad Prism 8. The sample size (n) refers to the number of mice from which the samples were harvested. Data are presented as the mean ± standard error of mean (SEM) and were analysed using the Turkey or Sidak t-test for multiple comparisons after analysis of variance (ANOVA). Image J was used to

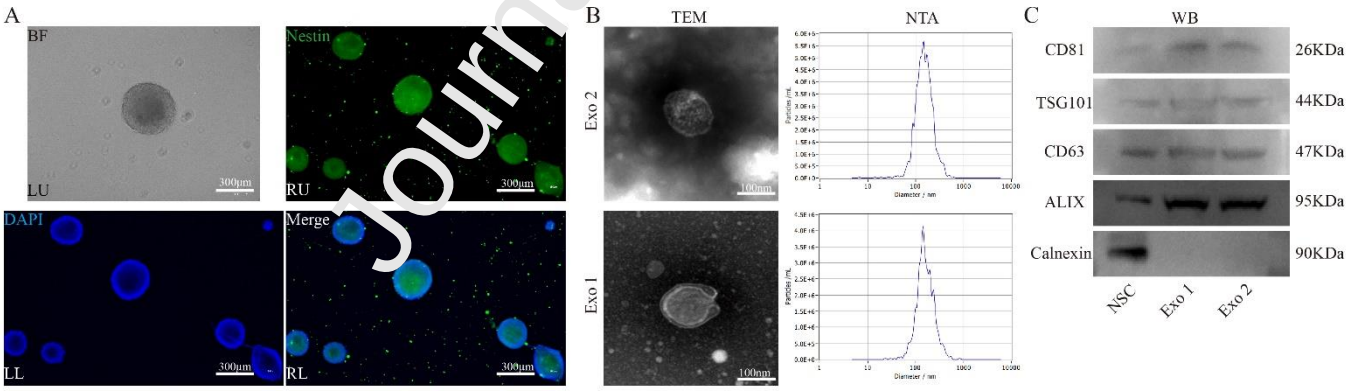

Figure 1 Identification of NSCs and exosomes. (A) The bright field (LU) and nestin$^+$ fluorescence of NSCs were observed (LU: bright field; RU: Nestin; LL: DAPI; RL: Merge). (B) The micro-structure of exosomes was detected by TEM. (C) The specific protein makers of exosomes were detected by WB. n = 3.

quantify the volume infarct and fluorescence intensity of the ischemic area. A p-value < 0.05 was considered significant.

Results & Discussion

Over the past decade, the number of studies evaluating the efficacy of NSCs, neurons, mesenchymal stem cells (MSCs), and neuro-related factors like brain-derived neurotrophic factor (BDNF) in post-apoplectic regeneration has grown exponentially (Salgado et al., 2015; Stonesifer et al., 2017). Post-apoplectic regeneration is a dynamic and complex process in which cells and the surrounding microenvironment interact to restore the structure of injured tissue (Shi et al., 2012).

In the past few decades, numerous biomaterial products have been developed and applied for neurogenesis and neuro-angiogenesis. Of these products, the porous hydrogel scaffold participates in nerve regeneration (El-Naggar et al., 2020; Yang et al., 2021).

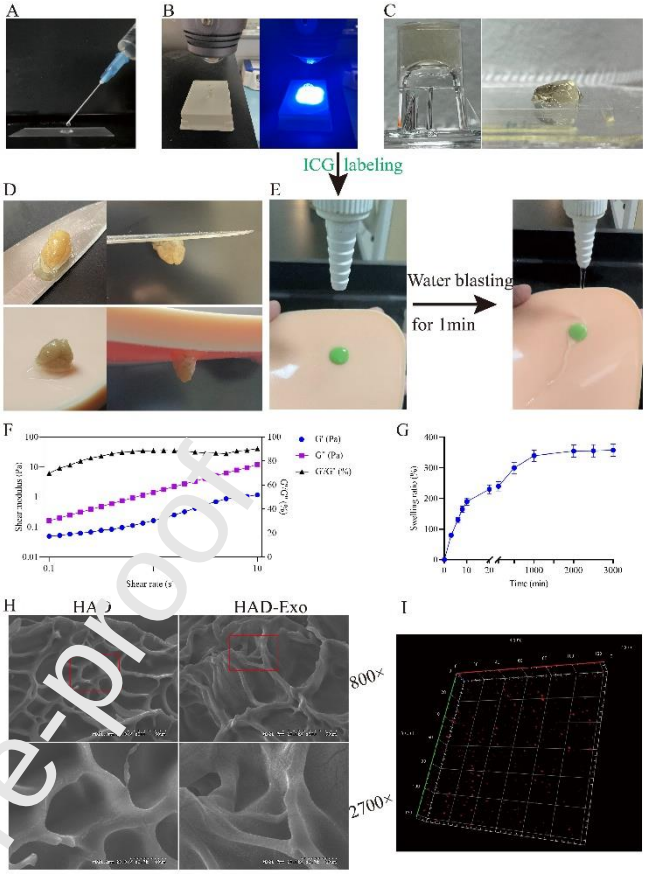

Figure 2 The ultrafast gelation and characteristics of HAD. (A) The syringeability of HAD hydrogel. (B) The procedure of photo-crosslinking of HAD precursor to HAD hydrogel in transwell cell. (C) The solidified HAD hydrogel in the inverted transwell cell, and the shape of HAD after removal from the transwell cell. (D) The adhesive properties of HAD to adhere to the iron material and artificial skin with brain tissue. (E) The adhesive properties to artificial skin of ICG labelled-HAD under water blasting for 1 min. The rheological properties (F) and swelling ratio (G) of HAD hydrogel. (H) The microporous structure of HAD (-Exo) and the distribution of exosomes in HAD-Exo complex. (I) The 3D images of distribution of exosomes in HAD-PKH26-Exo complex. n = 3.

As the main secreted component of the cellular matrix, HAD hydrogels can provide a physiological 3D structure in brain tissue (Shi et al., 2021; Warwar Damouny et al., 2022). This structure allows cellular interaction for proliferation, migration, and differentiation, thus promoting revascularization and neurogenesis. Due to the scavenging metabolism that occurs *in vivo*, the rate of migration of Exos into brain tissue is less using traditional injection (Guo et al., 2021). The biomaterials often have unique physical characteristics that decrease universal inflammation, cytotoxicity, and extensive scar formation (Fetz and Bowlin, 2022).

Identification of NSCs and Exos

Stem cell therapy, mainly using NSCs and MSCs, has become a hopeful approach for angiogenesis, neurogenesis, and tissue regeneration in recent years. NSCs have many advantages over MSC in nervous system applications. The safety and efficacy of NSCs have been confirmed in IS (Gasparetto et al., 2022). NSCs can directly differentiate into neurons or glial cells, which release various extracellular vesicles and accelerate the process of IS, including reducing apoptosis and oxidative stress, and promoting neuro-angiogenesis and neurogenesis (Sacco et al., 2018). NSCs have properties of self-renewal and multipotency, which allows the protracted generation of neurons and glia (Boese et al., 2018). Although NSCs are difficult to obtain and culture, their properties are homologous to neural cells and their rate of immunological rejection in brain tissues is low (Huang et al., 2018). Functions of NSCs involve multiple aspects, including cell replacement, angiogenesis, secretion of growth factors, activation of endogenous reparative pathways, and modulation of neuroinflammation (Sakata et al., 2012). The obtained NSCs displayed agglomerate growth and classical global-like morphology. These NSCs were identified by nestin with IF staining (**Fig. 1A**).

Extracellular vesicles or Exos have similar actions and are easier to obtain, allowing their encapsulation of biomaterials to deliver specific molecules, proteins, or RNAs for therapeutic effects. Extracellular vesicles derived from NSCs have a multimodal

action (Doeppner et al., 2018), which promotes proliferation of endogenous NSCs in the subventricular and subgranular zone, fosters synaptic growth and remodelling, and neuro-angiogenesis (Baker et al., 2019). In recent years, Exos have been considered a new form of therapy. SC derived Exos and biomaterials are considered effective strategies of neural restoration, and their combination therapy appears to produce organic outcomes.

The Exos were harvested from the supernate of NSCs by ultracentrifugation. TEM revealed the saucer-like structure of the Exos (**Fig. 1B**). NTA was adopted to assess the diameter size distribution and the particle concentration of Exos. Diameters ranged from 50 to 180 nm (**Fig. 1B**). WB results revealed that Exos expressed surface markers of Exos, including CD81, CD63, TSG101, and ALIX, and did not express the negative marker Calnexin (**Fig. 1C**). The collective data demonstrated the successful isolation of Exos.

Characteristics of HAD

Tissue engineering and regenerative medicine research have recently become a research hotspot approach, with the goal of facilitating the rejuvenation of injured brain tissue (Bartlett et al., 2020). Bioengineering technologies that utilize biomaterials, SCs, and biologically active factors have been widely studied in nerve system diseases (Daly et al., 2013). Numerous reports have implicated HA as a prospective biomaterial for encapsulating SCs or their derivatives to promote the regeneration of poorly vascularized tissues, such as epithelial, cartilage, bony, skin, cardiovascular, and adipose tissues (Prè et al., 2016). Through the modification of material properties, we added catecholamine branched chains to the HA main chain to incorporate it into a hydrogel precursor, which was adhered to tissues by ultraviolet irradiation. Hydrogels have multiple properties, including high water content, pliability, and a tissue-like 3D environment, which allow the encapsulation of Exos and cell adhesion at the target site (Gu et al., 2021; Shao et al., 2019). Lower concentration HAD hydrogels have a higher exosome encapsulation rate. In the

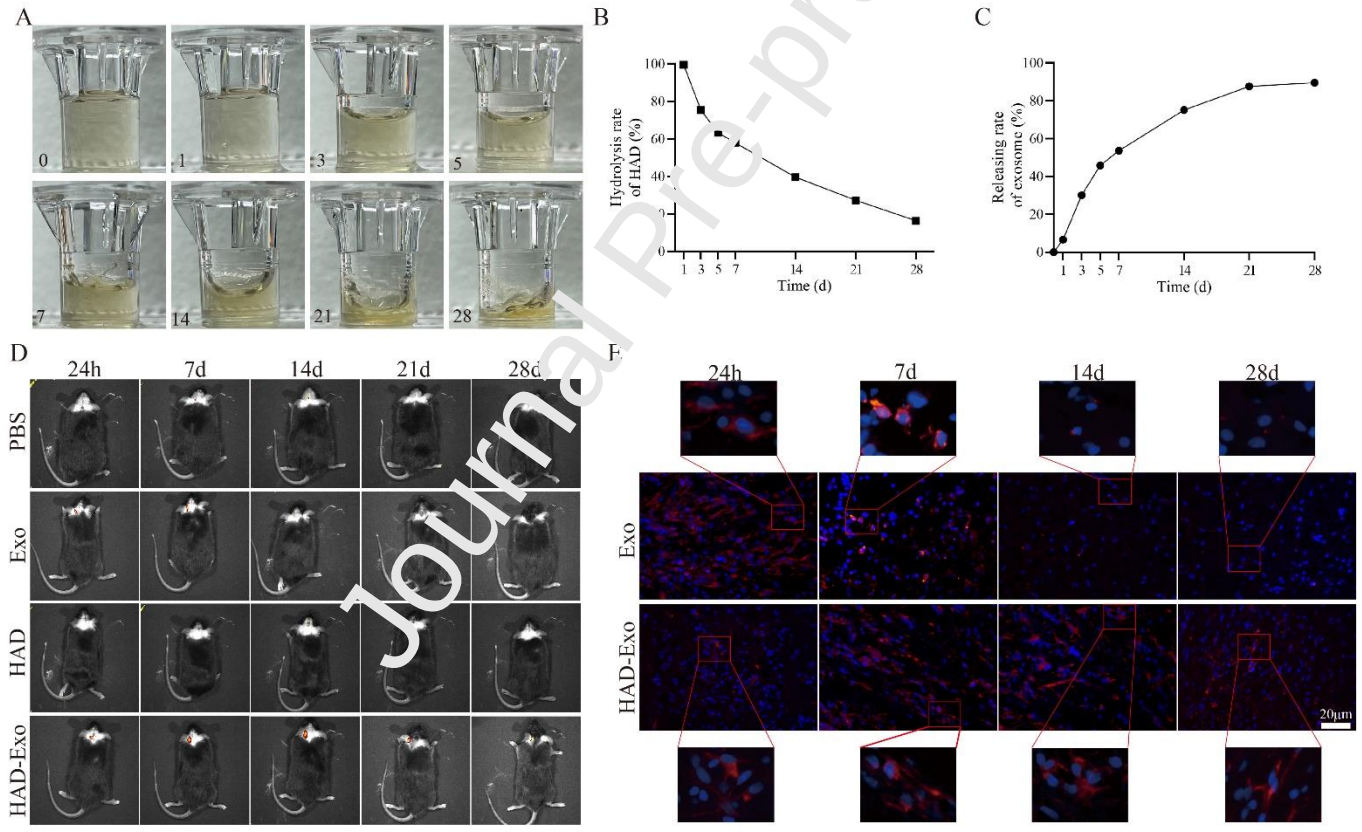

Figure 3 The hydrolysis of HAD-Exo and controlled release of Exos in vitro and in vivo. The hydrolysis of HAD with time by transwell hydrolysis test (A) and the quantitative analysis of hydrolysis and controlled release rate of HAD (B-C) in vitro. The controlled release situation of exosomes by IVIS in each groups in vivo. (E) The distribution of PHK26-Exos in injection area in brain tissues of Exo and HAD-Exo groups. PKH26-labelled Exo (red) and DAPI (blue, nucleus). n = 3 for each group.

present study, 3% HAD exhibited stable mechanical properties and low immunogenicity, and was chosen as the Exo carrier.

The adhesive property of HAD was evidenced by the capability to adhere to the iron material and artificial skin, and withstood the flow of deionized water (**Fig. 2D-E**). The storage modulus (G'') and loss modulus (G') were detected by rheometry. No intersection was observed between G' and G'' with the strain ranging from 1% to 100%, and the frequency ranging from 0.1 to 10 Hz. G'' was always higher than G' (**Fig. 2F**). The equilibrated swelling ratios of the HAD precursor exceeded 100% (**Fig. 2G**). The water uptake ability of the HAD hydrogel beneficially improved the microenvironment, which promoted angiogenesis and anti-

inflammation. Fluids exudated from necrotic cells could be absorbed and the incidence of abscess or porosis reduced. These results showed that the micro-network of HAD hydrogel did not collapse. The gel-like behaviour was maintained, corresponding the frequency and strain ranges.

Scanning electron microscope images of the formulations showed that HAD hydrogels lacking Exos had a microporous structure after freeze-drying. Exos encapsulated in HAD-Exo hydrogels were evenly distributed on the surface of microporous structure (**Fig. 2H**). The 3D images of HAD-PKH26-Exo obtained by laser scanning confocal microscopy similarly indicated that Exos were evenly distributed in HAD-Exo hydrogels (**Fig. 2I**).

The collective results provided further evidence that HAD hydrogels were injectable and underwent ultrafast gelation and proper mechanical properties, resulting in superior cellular derivative retention characteristics.

Controlled-release of HAD-Exo *in vivo* and *in vitro*

In this study, we constructed a combination of HAD and Exo, and applied the combination to a mouse MCAO model to validate the capacity of the combination treatment to prolong exosome maintenance. The HAD-Exo complex significantly promoted angiogenesis and maintained bioactivity of Exos. HAD-Exo treatment following IS achieved the long-term controlled release of Exos without multiple wounds. Transplantation of NSCs or their derivatives is an optimal choice. NSCs repair brain tissue post-IS by differentiating into neurons and also reduce infarct volume and blood-brain-barrier disruption by regulating the microenvironment, reducing inflammation, and promoting angiogenesis and neurogenesis (Hamblin et al., 2022). Our previous studies have shown that administration of NSC-derived Exos was more beneficial for accelerating nerve regeneration than NSCs themselves (Zhang et al., 2018a; Zhang et al., 2018b; Zhu et al., 2023). However, the low survival and rapid clearance rate are critical challenges for the application of Exos through the circulatory system.

The function of Exos mainly depends on their components consisting of DNA, RNA, proteins, and cellular factors. NSC-derived Exos also have a short residence time due to their rapid clearance *in vivo* (Xing et al., 2021). To attain a sustained treatment effect, multiple injection of Exos is required for IS. This increases the risk of infection in patients and laboratory animals. Therefore, increasing the retention time using biomaterials to deliver Exos represents a better strategy. Our results demonstrated that HAD hydrogel could be utilized to ensure a sustained and steady release of Exos *in vitro* (**Fig. 3A-C**) and *in vivo* (**Fig. 3D-E**).

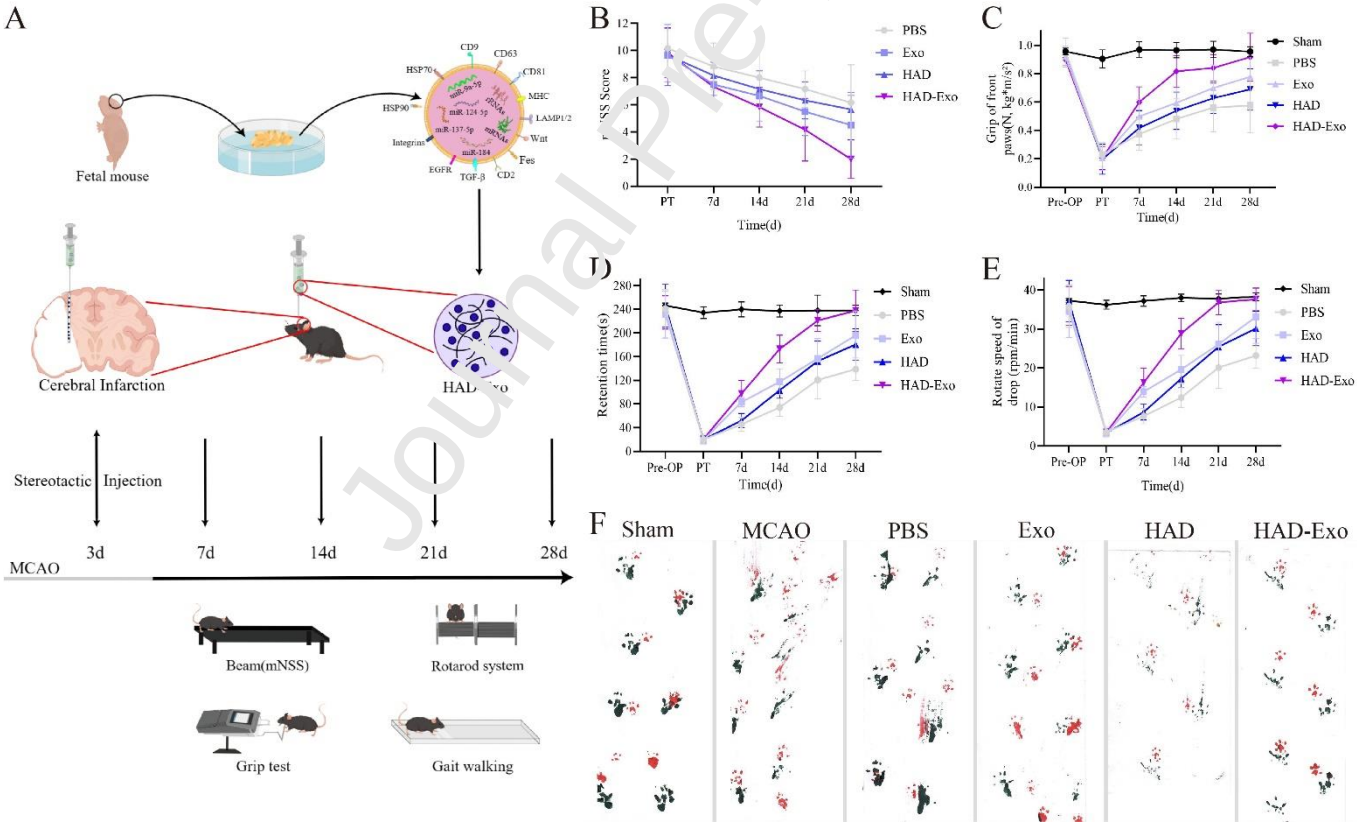

Figure 4 The schematic diagram of overall research, and the improvement of neurological function. (A) The schematic diagram of overall research. (B) The neurological improvement of each group by mNSS. The improvement of movement function of each group by grip of front paws (C), rotarod system (D-E) and Catwalk gait (F). n = 6 for each group.

The 3% HAD-Exo complex was chosen to test the release of Exos. *In vitro*, Exos encapsulated in HAD were released stably for a long time as catalysed by hyaluronidase to the lower chamber of the Transwell apparatus (**Fig. 3A**). The time-dependent relationship of HAD-Exo hydrolysis and Exo release is shown in **Fig. 3B-C**.

PKH26 is a lipophilic long-chain carbocyanine dye that is highly fluorescent with a long half-life. To detect the sustained release of Exos *in vivo*, Exos were labelled with PKH26 (PKH26-Exos) and encapsulated in 3% HAD. Monitoring the localization and migration of the HAD-PKH26-Exos allowed the evaluate of the contributions of the complex in the injection area. PBS/PKH26-Exo/HAD/HAD-PKH26-Exo were injected stereotactically into the ischemic junctional zone of mice. IVIS imaging revealed that the red fluorescent PKH26 (red fluorescence) began to gather around the injection hole 24 h later, and could still be detected until 28 days in the HAD-Exo group. PKH26-Exos without HAD displayed mass aggregation and partial migration around the injection site 24 h later, and less red fluorescence residual 14 days later (**Fig. 3D**). Fluorescence microscopy of harvested brain tissue revealed red fluorescence around the injection zone in the HAD-Exo group. Fluorescence could still be detected until 28 days. PKH26-Exo without HAD showed less red fluorescence on the day 14 (**Fig. 3E**).

Besides, the bilayer membrane structure of Exo is significant in retaining its function. The stability of exosomes released by HAD-Exo are analysed by NTA, WB and TEM, the results are displayed in supplementary materials (**Figure S1**). There is no difference of diameter or deformity of morphology between the released exosomes and the previous exosomes, and the surface protein has not changed, so it still retains biological activity.

These results revealed that 3% HAD-Exo could maintain the sustained release of Exos and ensure the effectiveness of Exos in the ischemic junctional area.

HAD-Exo improved the neurological function of MCAO mice

Nerve regeneration is a complicated and delicate process. Functional nerve regeneration has always been a great challenge for patients and clinicians. Nerve regeneration is complex and entails inflammation, angiogenesis, neurogenesis, tissue remodelling, and other factors (Lo et al., 2003). Decreasing pro-inflammatory cytokines and compromised neuro-vascularization might inhibit and delay nerve repair process. The mouse model of MCAO was created. These mice were injected stereotactically into the ischemic junctional zone with HAD-Exo, Exo, HAD, or PBS. The schematic diagram of the animal experimental procedure is shown in **Fig. 4A**.

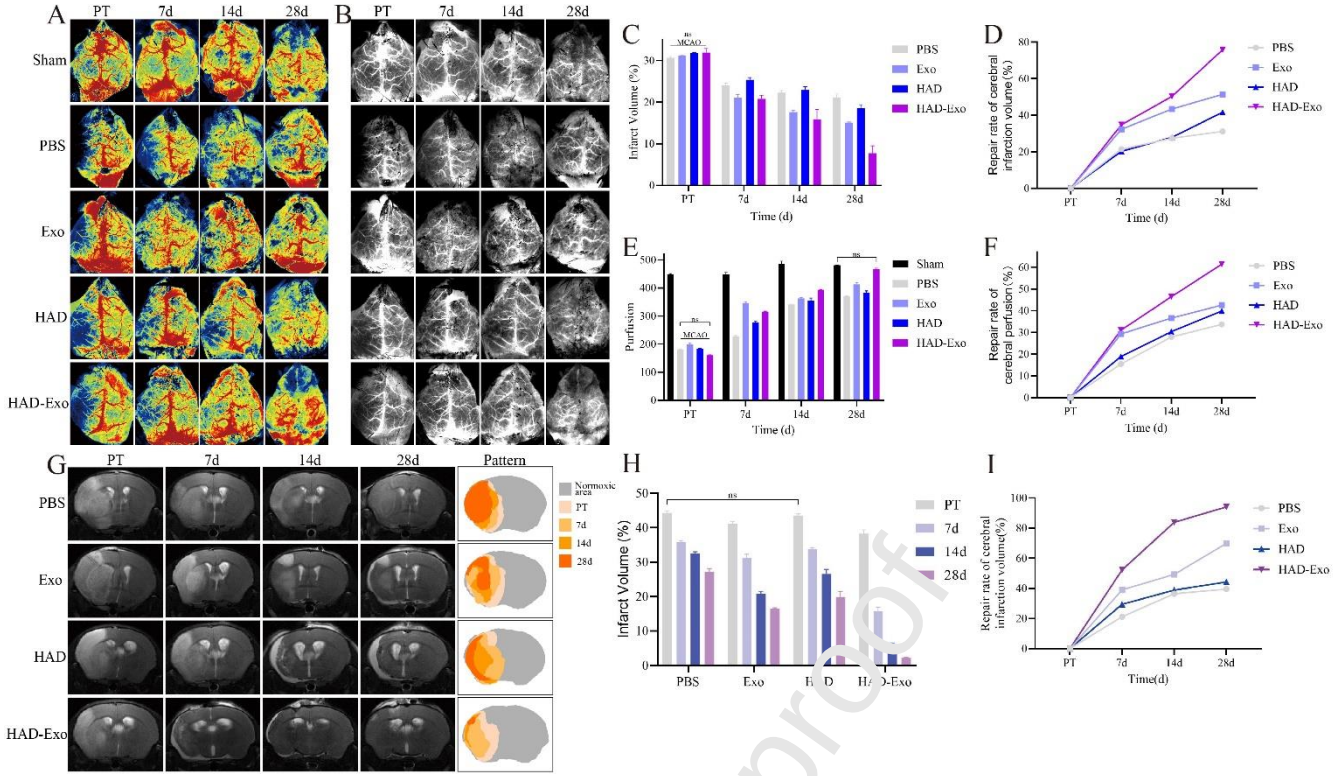

Figure 5 The improvement of cerebral angiogenesis and infarct volume by LSIS and MRI. The pseudo color (A) and greyscale (B) images of infarct volume following MCAO surgery in each group by LSIS. (C-D) The quantitative analysis and repair rate of infarct volume in each group by LSIS. (E-F) The quantitative analysis and repair rate of cerebral perfusion in each group by LSIS. ns: no significance; there were all statistically difference between other groups without "ns" labelled. (G) The images of variation of infarct volume following MCAO surgery in each group by MRI (Pattern images exhibited the variation of infarct volume by ImageJ software). (H-I) The quantitative analysis and repair rate of infarct volume in each group by MRI. * p-value < 0.05 vs PBS group, # p-value < 0.05 vs Exo group, & p-value < 0.05 vs HAD group. n = 6 for each group. In C, D, E, F, H and I data are shown as mean ± SEM.

The mNSS of the mice in each group at 0, 7, 14, 21, and 28 days are illustrated after MCAO. On day 28th after treatment, the neurological function with the HAD-Exos composite treatment was remarkably higher than PBS and HAD groups (HAD-Exo vs PBS: $p < 0.001$; HAD-Exo vs HAD: $p < 0.01$) (**Fig. 4B**). Compared to the PBS group, from the Pre-operation period (Pre-OP) to 28 days, the Exo, HAD, and HAD-Exo groups displayed improved muscle strength, as indicated by front paw grip strength. The HAD-Exo group recovered the fastest and displayed the highest strength. On day 7th, 14th, 21st and 28th after treatment, the muscle strength with the HAD-Exos composite treatment was remarkably higher than PBS and HAD groups (HAD-Exo vs PBS: $p < 0.001$; HAD-Exo vs HAD: $p < 0.05$) (**Fig. 4C**). The rotarod system was used to test fatigue resistance of motor function. The MCAO mice exhibited significant motor function deficits, which were most prominent 1−3 days after MCAO. As treatment intervention, sustained exercise capacity increased from 7 to 28 days. The HAD-Exo group showed significantly more durable exercise persistence capacity than other groups, including retention time and rotate speed of drop. On day 7th after treatment, the motor balance with the HAD-Exos composite treatment was remarkably higher than PBS and HAD groups (HAD-Exo vs PBS: $p < 0.01$; HAD-Exo vs HAD: $p < 0.05$). On day 14th, 21st and 28th after treatment, the motor balance with the HAD-Exos composite treatment was remarkably higher than PBS, Exo and HAD groups (HAD-Exo vs PBS: $p < 0.0001$; HAD-Exo vs Exo: $p < 0.05$; HAD-Exo vs HAD: $p < 0.001$) (**Fig. 4D-E**). The coordination of fore and hind paw movements decreased immediately after MCAO. Thus, gait analysis was used to assess the coordination of movements following treatment at 28 days. The HAD-Exo group displayed significantly improved motor coordination (HAD-Exo vs other groups: $p < 0.05$, **Fig. 4F**).

Collectively, the results demonstrated a significant effect of HAD-Exo on long-term recovery of motor function of MCAO mice. HAD-Exo could support maintenance and biological activity of Exos, and effectively accelerate neurological function recovery after IS.

HAD-Exo improved the cerebral angiogenesis and infarct volume

The prognosis of stroke in terms of neurological deficits and long-term disabilities is related to the area and size of brain damage (Lo et al., 2003). In the study, we applied PBS, Exo, HAD, and HAD-Exo to the ischemic area following MCAO. The HAD-Exo group displayed a better repair rate of infarct volume compared to the rates of the other groups during the whole repair process. LSIS of cerebral blood flow was performed in mice and MRI was used to assess cerebral angiogenesis and improvement of infarct volume.

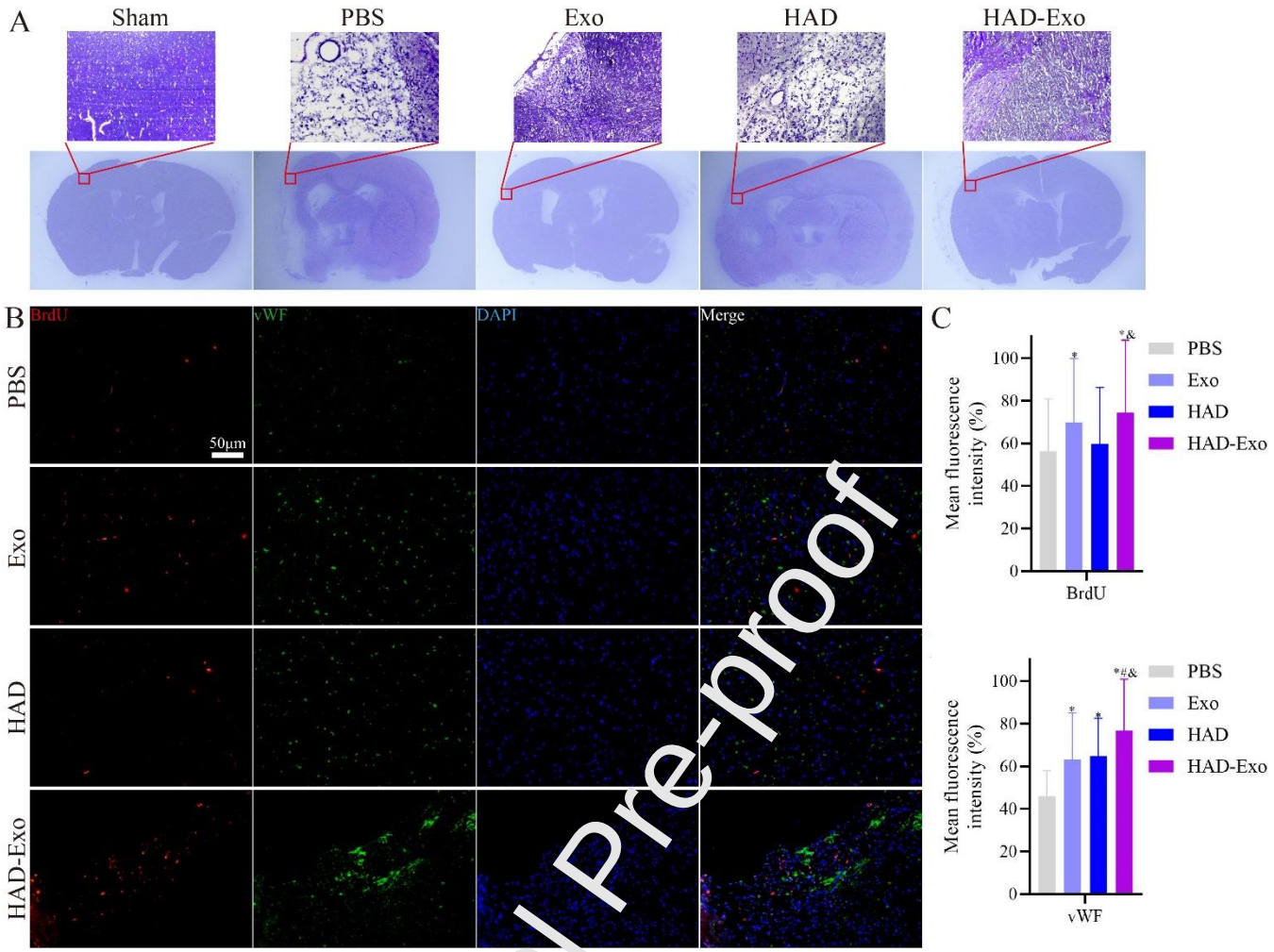

Figure 6 The improvement of cell proliferation and angiogenesis. (A) The representative images of Nissl staining on day 28th after MCAO. Bregma level: -0.5 to -0.1 mm. (B) BrdU/vWF staining of cell proliferation and angiogenesis in the ischemic area on day 28th after MCAO. (C-D) The mean fluorescence intensity of BrdU and vWF in the ischemic area on day 28th after MCAO. * p-value < 0.05 vs PBS group, # p-value < 0.05 vs Exo group, & p-value < 0.05 vs HAD group. 3 slides for per mouse, n = 6 for each group. In C and D data are shown as mean ± SEM.

LSIS revealed severe cerebral ischemia on the ischemic side. The ischemic area was hypoperfused after MCAO. With treatment intervention, cerebral blood perfusion gradually recovered, which was more obvious in HAD-Exo group at the same time (**Fig. 5A/B**). The variation of infarct volume of each group by LSIS was showed in **Fig. 5C**, and the line chart of repair rate of infarct volume was exhibited in **Fig. 5D**. The variation of cerebral perfusion of each group by LSIS was showed in **Fig. 5E**, and the line chart of repair rate of cerebral perfusion was exhibited in **Fig. 5F**. MRI revealed the similar size of cerebral infarct volume prior to treatment. With treatment intervention, the infarct volume was reduced gradually. The reduction in the HAD-Exo group was more significantly than other groups at the same timepoint, and the pattern images showed the variation of infarct volume by ImageJ software (**Fig. 5G**). The variation of infarct volume of each group by MRI was showed in **Fig. 5H**, and the line chart of repair rate of infarct volume was exhibited in **Fig. 5I**. The findings indicate that HAD-Exo can protect the biological activity of Exos, and can continuously release Exos, resulting in sustained, stable nerve repair.

HAD-Exo improved the neurovascular unit remodelling

Pathological assessment provided further evidence of the effects of HAD-Exo treatment on the recovery of neurological function recovery. Nissl staining revealed the infarct volume and neuron damage of brain tissues in the groups 28 days following treatment. A significant residual loss of brain tissue in the PBS group was observed. The infarct volume of brain tissue in the Exo group was repaired by 85%. Abnormal neurons and loose tissue were evident in the unrepaired region. The brain tissue was partially repaired. Many abnormal neurons and loose connective tissue were evident surrounding the unrepaired area in the HAD group. The infarct volume of the ischemic side was completely repaired in the HAD-Exo group. In this group, the abnormal neurons were significantly reduced, and the connective tissue was dense. Collectively, compared to PBS group, the infarct volume and neuron damage of brain tissues of ischemic side was significantly improved in the other three groups, while the improvement of the HAD-Exo group was greatest (**Fig. 6A**).

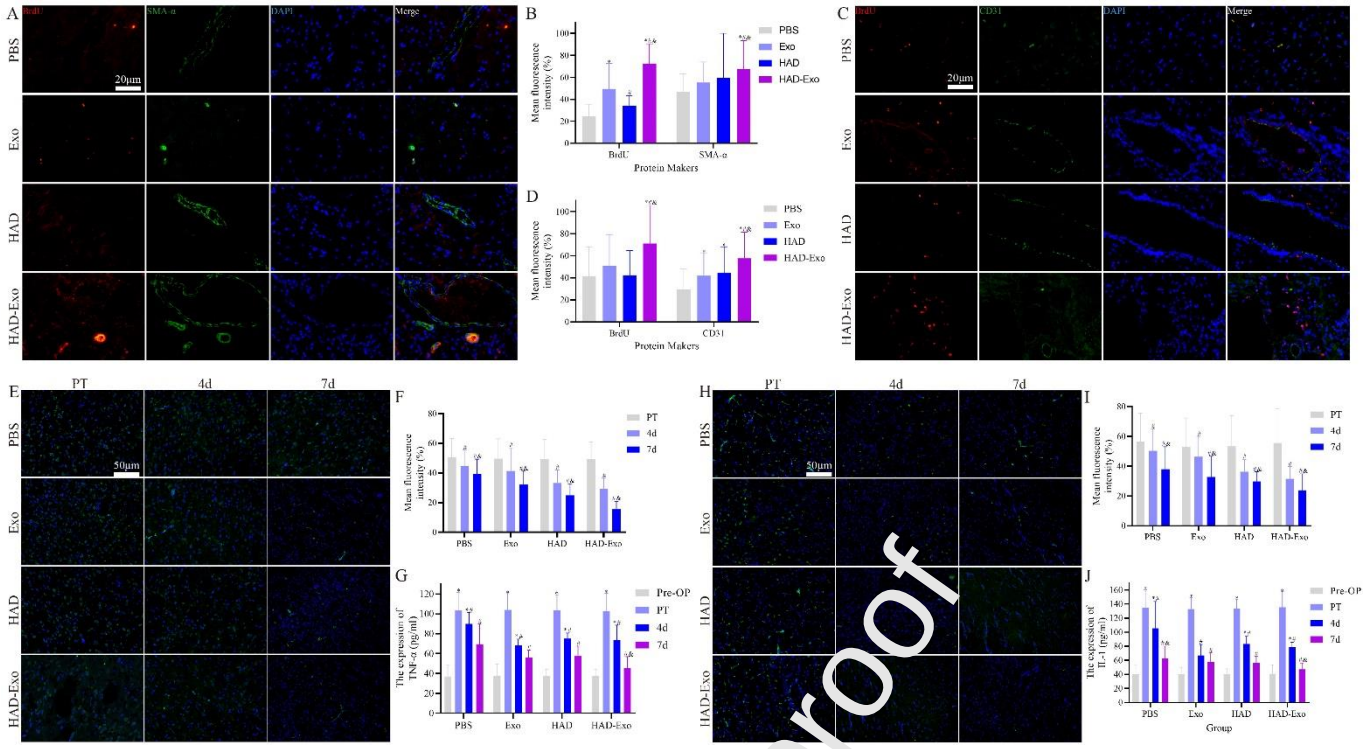

Figure 7 The IF staining of diverse micro-vessel proteins, and the inflammatory response in vivo. (A) SMA-α staining of myofibroblasts in the ischemic area on day 28th after MCAO. (B) Quantification of SMA-α stained tissues. (C) Representative images of IF staining of CD31 on day 28th in the ischemic area. (D) Micro-vessel density analyses of diverse treatment groups on the day 28th. * p-value < 0.05 vs PBS group, # p-value < 0.05 vs Exo group, & p-value < 0.05 vs HAD group (B and D data). 3 slides for per mouse, n = 6 for each group. (E) TNF-α staining of pro-inflammatory factor in the ischemic area on the acute phase after MCAO. (F) Quantification of TNF-α stained tissues. (G) The expression of TNF-α in blood of each group. (H) IL-1 staining of pro-inflammatory factor in the ischemic area on the acute phase after MCAO. (I) Quantification of IL-1 stained tissues. (J) The expression of IL-1 in blood of each group. * p-value < 0.05 vs Pre-OP, # p-value < 0.05 vs PT, & p-value < 0.05 vs 4d (F, G, I and J data). n = 6 for each group. In B, D, F, G, I and J data are shown as mean ± SEM.

We also assessed the micro-angiogenesis/capillary formation in the ischemic area. Markers of micro-angiogenesis (vWF) and cell proliferation (BrdU) were detected via IF staining. Similar fluorescence intensity was evident for vWF in the Exo and HAD groups, indicating similar effects on overall angiogenesis in the groups. However, the fluorescence intensity of BrdU in the Exo group was higher than that in the HAD group, indicating that Exo could promote greater proliferation of nerve cells in brain tissue. Furthermore, the fluorescence intensities of BrdU and vWF of the HAD-Exo group were significantly higher than that of other groups, indicating that the combination of HAD-Exo promoted cell proliferation and micro-angiogenesis more than treatment with Exo or HAD alone (**Fig. 6B-D**). The infarct volume of the ischemic side was completely repaired in the HAD-Exo group, abnormal neurons were significantly reduced, and the connective tissue was dense.

Furthermore, the increased expression of SMA-α and CD31 indicated that both HAD-Exo could promote myofibroblast formation and vascular endothelium effectively, indicating that HAD provided a suitable 3D microenvironment of brain tissue. To explore the potential therapeutic mechanisms of the local application of Exo, HAD, and HAD-Exo on angiogenesis, we performed IF staining of BrdU, CD31, and SMA-α in the ischemic area after 28 days of treatment. BrdU was used to determine total cell proliferation. The number of BrdU positive cells in the HAD-Exo and Exo groups significantly increased compared to other groups. Following the HAD-Exo and HAD treatments, higher expression of the myofibroblast marker SMA-α was detected compared to the other groups (**Fig. 7A-B**). Expression of endothelial cell marker CD31 was used to assess newly formed vessels in regenerated tissue. The HAD and Exo groups had similarly remarkable blood vessel numbers, in contrast with the PBS group after 28 days of treatment (**Fig. 7C-D**). Furthermore, the HAD-Exo group displayed significantly more blood than the other three groups.

HAD-Exo decreased the inflammation without tissue toxicity

Growing evidence points to the importance of TNF-α and IL-1 pro-inflammatory factor in IS inflammation (Wang et al., 2007). IL-1 mediates ischemic, traumatic and excitotoxic brain injury, probably through multiple effects on neurons, vasculature and glia. TNF-α might contribute to neuronal injury (Allan and Rothwell, 2001). IF staining of TNF-α and IL-1 of ischemic area in each group was performed, the results are shown in **Fig. 7E/H**, respectively. The quantitative analysis of IF intensity is presented in **Fig. 7F/I**, respectively. Following stereotactic injection on day 3 in the MCAO model, compared with PT, the improvement of TNF in each group was statistically different on day 4 and 7, with the improvements being most notable in the HAD and HAD-Exo groups. Similarly, compared with PT, the improvement of the pro-inflammatory factor IL-1 in each group, except the Exo group, was statistically significantly different on day 4. The improvement of the HAD-Exo group was the most significant. Compared with PT,

the improvement of IL-1 in the HAD and HAD-Exo groups was statistically significantly different on day 7. The improvement of

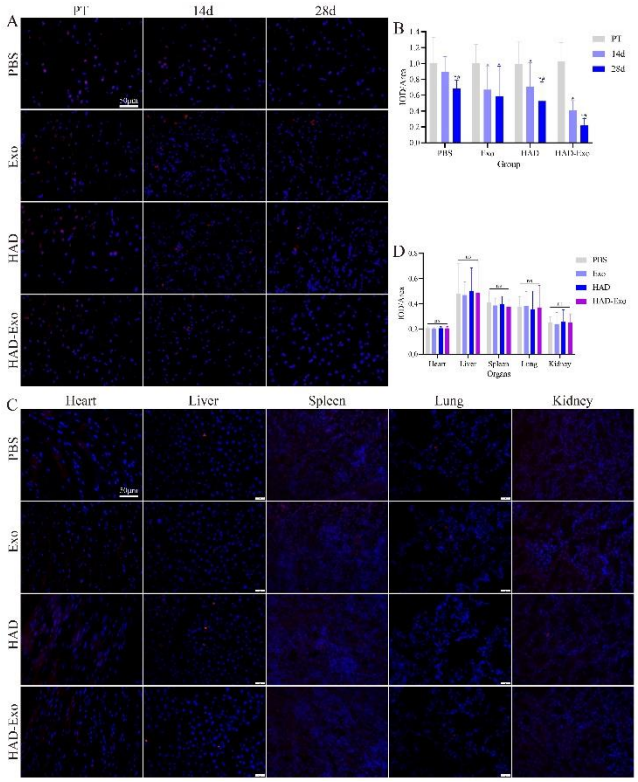

Figure 8 The safety assessment of HAD/HAD-Exo injection. (A) TUNEL staining of brain tissues of each group with time. (B) Quantification of apoptotic cells (red) i stained brain tissues (* p-value < 0.05 vs PT, # p-value < 0.05 vs 14d). (C) TUNE staining of other organ tissues of each group. (D) Quantification of apoptotic cells (red) in stained organ tissues (ns: no significance; there were no statistical differences in each organ group). 3 slides for per mouse, n = 6 for each group. In B and D data are shown as mean ± SEM.

the HAD-Exo group remained the most obvious.

The acute phases of IS begin with inflammation. Cerebral ischemia is followed by an inflammatory reaction induced by various injured cells, which can continue for days to weeks after the ischemia. It is now universally accepted that such inflammatory processes contribute to the progression of ischemic brain injury and to the exacerbation of focal neurological deficits. Cytokines, including IS, are released in the brain after insults and are expressed in cells of the immune system. In addition, production by resident brain cells, including neurons and glia, has been observed (Liu et al., 1994; Sairanen et al., 2001). The most studied cytokines related to pro-inflammation in stroke are IL-1 (Haqqani et al., 2005), and TNF-α (Han and Yenari, 2003). IL-1 and TNF-α appear to exacerbate cerebral injury. In the acute phase of MCAO, the high expression of IL-1 and TNF has been documented within 12 h following ischemia and at later times (24–72 h). These findings indicate biphasic expression and continued high expression lasting several days (3–7 days). The ELISA results revealed that compared to the Pre-OP period, TNF-α and IL-1 plasma proteins were significantly increased at the PT timepoint. Compared with the PBS treatment group, the protein expressions of TNF and IL-1 in the Exo, HAD, and HAD-Exo groups decreased to varying degrees after stereotactic injection ($p<0.05$). The decrease degree of the Exo and HAD-Exo groups was most notable on day 4 and 7, respectively (**Fig. 7G/J**). These results revealed that the HAD group partially inhibited inflammation in plasma, with the anti-inflammatory effect of Exos being more dominant. The expressions of pro-inflammatory factors in plasma deceased significantly and were related the number of effective Exos released. A single application of Exos had a short-term and limited effect on the inhibition of pro-inflammatory factors in plasma, with most Exos cleared by the body. However, in the HAD-Exo group, controlled release of Exos continuously inhibited body damage of pro-inflammatory factors in plasma.

To further assess the safety of stereotactic injection of HAD and HAD-Exo *in vivo*, TUNEL staining was performed to detect the damage of important organs of mice in each group, including brain, heart, liver, spleen, lung and kidney. Before treatment after MCAO surgery, a large number of apoptotic cells (red) appeared on the infarct side of the brain. With the advancement of treatment, compared to the PBS group, the Exo, HAD, and HAD-Exo groups all improved significantly. Among them, the degree of improvement of the HAD group was the lowest, and that of HAD-Exo group was the most significant (**Fig. 8A-B**). These results

indicated that exosomes might play a decisive role on the process of rescuing apoptotic cells of the brain tissue, and that the HAD-Exo complex plays an auxiliary role through the sustained release of Exos, allowing their maximum performance. In addition, no statistically significant difference in the mean fluorescence intensity of the examined organs, except brain, was evident in each group (**Fig. 8C-D**). These findings indicated that the injection of HAD or HAD-Exo into the body did not damage to the important organs, and that toxicity to the body was negligible.

Conclusions

In the present study, we successfully utilized NSC-derived Exos encapsulated in a HAD hydrogel for IS. The HAD-Exo complex maintained the biological activity of Exos, enhanced cell proliferation, angiogenesis, and anti-inflammation at the ischemic area, and improved the cerebral infarct and neurological function. HAD hydrogel as a delivery scaffold was suitable for delivering and releasing Exos continuously at the ischemic area. Compared to the Exo treatment, the HAD-Exo combination topically reduced dosing frequency and optimized the application process for IS. Our study showed that topically injected HAD-Exo complex was a promising alternative strategy for clinical translation of IS.

Abbreviations

IS: ischemic stroke; SCs: stem cells; NSCs: neural stem cells; Exo: exosome; miRNA: micro RNA; 3D: three-dimensional; HAD: modified hyaluronic acid; PFA: paraformaldehyde; DAPI: 4', 6-diamidino-2-phenylindole; IF: immunofluorescence; TEM: transmission electron microscope; NTA: nanoparticle tracing analysis; WB: western blotting; ELISA: enzyme-linked immunosorbent assay; HA: hyaluronic acid; DA: 3,4-dihydroxy-phenylalanine; AEMA: 2-aminoethyl methacrylate; EDC: 1-(3-Dimethylaminopropyl)-3-ethylcarbodiimide hydrochloride; NHS: N-Hydroxy succinimide; SR: swelling ratio; CCA: common carotid artery; ECA: external carotid artery; ICA: internal carotid artery; MCAO: middle cerebral artery occlusion; mNSS: modified Neurological Severity Score; LSIS: Laser speckle imaging system; MRI: magnetic resonance imaging; SEM: standard error of mean; Pre-OP: pre-operation; PT: pre-treatment; MSCs: mesenchymal stem cells; BDNF: brain-derived neurotrophic factor.

Ethics approval and consent to participate

All animal experiments are followed with the ARRIVE guidelines (see in the attachment). All authors stated that studies involving animals, not including client-owned animals. The experiments (Neural Stem Cell Derived Exosomes as Endogenous carrier for Ischemic Stroke model) were approved by the Animal Research Ethics Committee of Southeast University (approval number: 20210405006; approval date: 2021.04.05).

Author Contributions

All the authors read and approved the final manuscript. Conceptualization and Funding acquisition: LC, YW and J Long. Data curation: CG, YL, J Liu and WD. Formal analysis: WA and YH. Investigation: CG, YL and J Liu. Methodology: SL and TF. Project administration: CG, YL, J Liu, QZ and WD. Software: YL and JH. Validation: J Long, HC and YH. Writing-review & editing: J Long, YQ and YH. Writing-original draft & Figures: J Liu, CG and YL.

Conflicts of interest

There are no conflicts to declare.

Funding

This work was sponsored by National Key R&D Program of China (2022YFA1104900 & 2022YFA1104904 to LC), National Natural Science Foundation of China (32271423 to YW), Natural Science Foundation of Guangdong Province (2021A1515010013 to LC), Department of Education of Guangdong Province (2021ZDZX2011 to LC), Traditional Chinese Medicine Bureau of Guangdong Province (20221275 to LC), Guangzhou Municipal Science and Technology Project (202201011760 to LC) and President Foundation of Integrated Hospital of Traditional Chinese Medicine of Southern Medical University (1202101003 to LC & 1202103007 to J Long). The funding body played no role in the design of the study and collection, analysis, and interpretation of data and in writing the manuscript.

Acknowledgements

We thank Fig.Draw (https://www.figdraw.com/) for editing Graphical Abstract and Figure 4. We thank International Science Editing (http://www.internationalscienceediting.com) for polishing this manuscript (Code: 39859-BJUITQJ5O2).

References

Adams, H.P., Jr., del Zoppo, G., Alberts, M.J., Bhatt, D.L., Brass, L., Furlan, A., Grubb, R.L., Higashida, R.T., Jauch, E.C., Kidwell, C., Lyden, P.D., Morgenstern, L.B., Qureshi, A.I., Rosenwasser, R.H., Scott, P.A., Wijdicks, E.F., American Heart, A., American Stroke Association Stroke, C., Clinical Cardiology, C., Cardiovascular, R., Intervention, C., Atherosclerotic Peripheral Vascular, D., Quality of Care Outcomes in Research Interdisciplinary Working, G., 2007. Guidelines for the early management of adults with ischemic stroke: a guideline from the American Heart Association/American Stroke Association Stroke Council, Clinical Cardiology Council, Cardiovascular Radiology and Intervention Council, and the Atherosclerotic Peripheral Vascular Disease and Quality of Care Outcomes in Research Interdisciplinary Working Groups: the American Academy of Neurology affirms the value of this guideline as an educational tool for neurologists. Stroke 38, 1655-1711.

Allan, S.M., Rothwell, N.J., 2001. Cytokines and acute neurodegeneration. Nature reviews. Neuroscience 2, 734-744.

Baker, E.W., Kinder, H.A., West, F.D., 2019. Neural stem cell therapy for stroke: A multimechanistic approach to restoring neurological function. Brain Behav 9, e01214.

Bartlett, R.D., Eleftheriadou, D., Evans, R., Choi, D., Phillips, J.B., 2020. Mechanical properties of the spinal cord and brain: Comparison with clinical-grade biomaterials for tissue engineering and regenerative medicine. Biomaterials 258, 120303.

Boese, A.C., Le, Q.E., Pham, D., Hamblin, M.H., Lee, J.P., 2018. Neural stem cell therapy for subacute and chronic ischemic stroke. Stem Cell Res Ther 9, 154.

Chen, L., Zhang, G., Feng, S., Xue, M., Cai, J., Chen, L., Deng, Y., Wang, Y., 2022. Preparation and quality control standard of clinical-grade neural progenitor/precursor cells-derived exosomes (2022 China version). Journal of Neurorestoratology 10, 100001.

Contreras, E., Bolívar, S., Navarro, X., Udina, E., 2022. New insights into peripheral nerve regeneration: The role of secretomes. Exp Neurol 354, 114069.

Cook, D.J., Nguyen, C., Chun, H.N., L Llorente, I., Chiu, A.S., Machnicki, M., Zarembinski, T.I., Carmichael, S.T., 2017. Hydrogel-delivered brain-derived neurotrophic factor promotes tissue repair and recovery after stroke. Journal of Cerebral Blood Flow & Metabolism 37, 1030-1045.

Coscia, M., Wessel, M.J., Chaudary, U., Millán, J.D.R., Micera, S., Guggisberg, A., Vuadens, P., Donoghue, J., Birbaumer, N., Hummel, F.C., 2019. Neurotechnology-aided interventions for upper limb motor rehabilitation in severe chronic stroke. Brain 142, 2182-2197.

Daly, W.T., Knight, A.M., Wang, H., de Boer, R., Giusti, G., Dadsetan, M., Spinner, R.J., Yaszemski, M.J., Windebank, A.J., 2013. Comparison and characterization of multiple biomaterial conduits for peripheral nerve repair. Biomaterials 34, 8630-8639.

Darling, N.J., Xi, W., Sideris, E., Anderson, A.R., Pong, C., Carmichael, S.T., Segura, T., 2020. Click by Click Microporous Annealed Particle (MAP) Scaffolds. Advanced Healthcare Materials 9, 1901391.

Doeppner, T.R., Bähr, M., Giebel, B., Hermann, D.M., 2018. Immunological and non-immunological effects of stem cell-derived extracellular vesicles on the ischaemic brain. Ther Adv Neurol Disord 11, 1756286418789326.

El-Naggar, M.E., Othman, S.I., Allam, A.A., Morsy, O.M., 2020. Synthesis, drying process and medical application of polysaccharide-based aerogels. Int J Biol Macromol 145, 1115-1128.

Fetz, A.E., Bowlin, G.L., 2022. Neutrophil Extracellular Traps: Inflammation and Biomaterial Preconditioning for Tissue Engineering. Tissue Eng Part B Rev 28, 437-450.

Gasparetto, C., Schiller, G.J., Tuchman, S.A., Callander, N.S., Baljevic, M., Lentzsch, S., Rossi, A.C., Kotb, R., White, D., Bahlis, N.J., Chen, C.I., Sutherland, H.J., Madan, S., LeBlanc, R., Sebag, M., Venner, C.P., Bensinger, W.I., Biran, N., Ammu, S., Ben-Shahar, O., DeCastro, A., Van Domelen, D., Zhou, T., Zhang, C., Bentur, O.S., Shah, J., Shacham, S., Kauffman, M., Lipe, B., 2022. Once weekly selinexor, carfilzomib and dexamethasone in carfilzomib non-refractory multiple myeloma patients. British journal of cancer 126, 718-725.

Genet, N., Hirschi, K.K., 2021. Understanding neural stem cell regulation in vivo and applying the insights to cell therapy for strokes. Regen Med 16, 861-870.

Gu, C., Feng, J., Waqas, A., Deng, Y., Zhang, Y., Chen, W., Long, J., Huang, S., Chen, L., 2021. Technological Advances of 3D Scaffold-Based Stem Cell/Exosome Therapy in Tissues and Organs. Frontiers in Cell and Developmental Biology 9.

Gu, C., Liu, J., Li, Y., Zhang, Q., Lin, C., Huang, J., Duan, W., Deng, Y., Ahmed, W., Li, R., Long, J., Khan, A.A., Chen, L., 2022. Comparison of ketamine/xylazine and isoflurane anesthesia on the establishment of mouse middle cerebral artery occlusion model. Experimental Animals advpub.

Guo, L., Huang, Z., Huang, L., Liang, J., Wang, P., Zhao, L., Shi, Y., 2021. Surface-modified engineered exosomes attenuated cerebral ischemia/reperfusion injury by targeting the delivery of quercetin towards impaired neurons. Journal of nanobiotechnology 19, 141.

Hamblin, M.H., Murad, R., Yin, J., Vallim, G., Lee, J.P., 2022. Modulation of gene expression on a transcriptome-wide level following human neural stem cell transplantation in aged mouse stroke brains. Exp Neurol 347, 113913.

Han, H.S., Yenari, M.A., 2003. Cellular targets of brain inflammation in stroke. Current opinion in investigational drugs (London, England : 2000) 4, 522-529.

Haqqani, A.S., Nesic, M., Preston, E., Baumann, E., Kelly, J., Stanimirovic, D., 2005. Characterization of vascular protein expression patterns in cerebral ischemia/reperfusion using laser capture microdissection and ICAT-nanoLC-MS/MS. Faseb j 19, 1809-1821.

Huang, H., Qian, K., Han, X., Li, X., Zheng, Y., Chen, Z., Huang, X., Chen, H., 2018. Intraparenchymal Neural Stem/Progenitor Cell Transplantation for Ischemic Stroke Animals: A Meta-Analysis and Systematic Review. Stem Cells Int 2018, 4826407.

Johnstone, R.M., Adam, M., Hammond, J.R., Orr, L., Turbide, C., 1987. Vesicle formation during reticulocyte maturation. Association of plasma membrane activities with released vesicles (exosomes). J Biol Chem 262, 9412-9420.

Ju, R., Wen, Y., Gou, R., Wang, Y., Xu, Q., 2014. The experimental therapy on brain ischemia by improvement of local angiogenesis with tissue engineering in the mouse. Cell Transplant 23 Suppl 1, S83-95.
Lin, D.J., Cloutier, A.M., Erler, K.S., Cassidy, J.M., Snider, S.B., Ranford, J., Parlman, K., Giatsidis, F., Burke, J.F., Schwamm, L.H., Finklestein, S.P., Hochberg, L.R., Cramer, S.C., 2019. Corticospinal Tract Injury Estimated From Acute Stroke Imaging Predicts Upper Extremity Motor Recovery After Stroke. Stroke 50, 3569-3577.
Liu, T., Clark, R.K., McDonnell, P.C., Young, P.R., White, R.F., Barone, F.C., Feuerstein, G.Z., 1994. Tumor necrosis factor-alpha expression in ischemic neurons. Stroke 25, 1481-1488.
Llorente, V., Velarde, P., Desco, M., Gómez-Gaviro, M.V., 2022. Current Understanding of the Neural Stem Cell Niches. Cells 11.
Lo, E.H., Dalkara, T., Moskowitz, M.A., 2003. Mechanisms, challenges and opportunities in stroke. Nature reviews. Neuroscience 4, 399-415.
Long, J., Gu, C., Zhang, Q., Liu, J., Huang, J., Li, Y., Zhang, Y., Li, R., Ahmed, W., Zhang, J., Khan, A.A., Cai, H., Hu, Y., Chen, L., 2023. Extracellular vesicles from medicated plasma of Buyang Huanwu decoction-preconditioned neural stem cells accelerate neurological recovery following ischemic stroke. Frontiers in Cell and Developmental Biology 11.
Lyu, Z., Park, J., Kim, K.M., Jin, H.J., Wu, H., Rajadas, J., Kim, D.H., Steinberg, G.K., Lee, W., 2021. A neurovascular-unit-on-a-chip for the evaluation of the restorative potential of stem cell therapies for ischaemic stroke. Nat Biomed Eng 5, 847-863.
Mendelson, S.J., Prabhakaran, S., 2021. Diagnosis and Management of Transient Ischemic Attack and Acute Ischemic Stroke: A Review. Jama 325, 1088-1098.
Obernier, K., Alvarez-Buylla, A., 2019. Neural stem cells: origin, heterogeneity and regulation in the adult mammalian brain. Development 146.
Orellana-Urzúa, S., Rojas, I., Líbano, L., Rodrigo, R., 2020. Pathophysiology of Ischemic Stroke: Role of Oxidative Stress. Curr Pharm Des 26, 4246-4260.
Prè, E.D., Conti, G., Sbarbati, A., 2016. Hyaluronic Acid (HA) Scaffolds and Multipotent Stromal Cells (MSCs) in Regenerative Medicine. Stem Cell Rev Rep 12, 664-681.
Reed, S.L., Escayg, A., 2021. Extracellular vesicles in the treatment of neurological disorders. Neurobiol Dis 157, 105445.
Rong, Y., Liu, W., Wang, J., Fan, J., Luo, Y., Li, L., Kong, F., Chen, J., Tang, P., Cai, W., 2019. Neural stem cell-derived small extracellular vesicles attenuate apoptosis and neuroinflammation after traumatic spinal cord injury by activating autophagy. Cell Death Dis 10, 340.
Sacco, R., Cacci, E., Novarino, G., 2018. Neural stem cells in neuropsychiatric disorders. Curr Opin Neurobiol 48, 131-138.
Sairanen, T., Carpén, O., Karjalainen-Lindsberg, M.L., Paetau, A., Turpeinen, U., Kaste, M., Lindsberg, P.J., 2001. Evolution of cerebral tumor necrosis factor-alpha production during human ischemic stroke. Stroke 32, 1750-1758.
Sakata, H., Niizuma, K., Yoshioka, H., Kim, G.S., Jung, J.E., Katsu, M., Narasimhan, P., Maier, C.M., Nishiyama, Y., Chan, P.H., 2012. Minocycline-preconditioned neural stem cells enhance neuroprotection after ischemic stroke in rats. J Neurosci 32, 3462-3473.
Salgado, A.J., Sousa, J.C., Costa, B.M., Pires, A.O., Mateus-Pinheiro, A., Teixeira, F.G., Pinto, L., Sousa, N., 2015. Mesenchymal stem cells secretome as a modulator of the neurogenic niche: basic insights and therapeutic opportunities. Front Cell Neurosci 9, 249.
Shao, C., Liu, Y., Chi, J., Wang, J., Zhao, Z., Zhao, Y., 2019. Responsive Inverse Opal Scaffolds with Biomimetic Enrichment Capability for Cell Culture. Research (Washington, D.C.) 2019, 9783793.
Sharma, H.S., Chopp, M., Chen, L., Sarnowska, A., Xue, M., Ao, Q., Siniscalco, D., Chen, L., Hawamdeh, Z., Huang, H., 2022. The 2021 yearbook of neurorestoratology. Journal of Neurorestoratology 10, 100008.
Shi, W., Fang, F., Kong, Y., Greer, S.E., Kuss, M., Liu, B., Xue, Y., Jiang, X., Lovell, P., Mohs, A.M., Dudley, A.T., Li, T., Duan, B., 2021. Dynamic hyaluronic acid hydrogel with covalent linked gelatin as an anti-oxidative bioink for cartilage tissue engineering. Biofabrication 14.
Shi, W., Nie, D., Jin, G., Chen, W., Xia, L., Wu, X., Su, X., Xu, X., Ni, L., Zhang, X., Zhang, X., Chen, J., 2012. BDNF blended chitosan scaffolds for human umbilical cord MSC transplants in traumatic brain injury therapy. Biomaterials 33, 3119-3126.
Stonesifer, C., Corey, S., Ghanekar, S., Diamandis, Z., Acosta, S.A., Borlongan, C.V., 2017. Stem cell therapy for abrogating stroke-induced neuroinflammation and relevant secondary cell death mechanisms. Prog Neurobiol 158, 94-131.
Tsao, C.W., Aday, A.W., Almarzooq, Z.I., Anderson, C.A.M., Arora, P., Avery, C.L., Baker-Smith, C.M., Beaton, A.Z., Boehme, A.K., Buxton, A.E., Commodore-Mensah, Y., Elkind, M.S.V., Evenson, K.R., Eze-Nliam, C., Fugar, S., Generoso, G., Heard, D.G., Hiremath, S., Ho, J.E., Kalani, R., Kazi, D.S., Ko, D., Levine, D.A., Liu, J., Ma, J., Magnani, J.W., Michos, E.D., Mussolino, M.E., Navaneethan, S.D., Parikh, N.I., Poudel, R., Rezk-Hanna, M., Roth, G.A., Shah, N.S., St-Onge, M.-P., Thacker, E.L., Virani, S.S., Voeks, J.H., Wang, N.-Y., Wong, N.D., Wong, S.S., Yaffe, K., Martin, S.S., 2023. Heart Disease and Stroke Statistics—2023 Update: A Report From the American Heart Association. Circulation 147.
Wang, Q., Tang, X.N., Yenari, M.A., 2007. The inflammatory response in stroke. J Neuroimmunol 184, 53-68.
Warwar Damouny, C., Martin, P., Vasilyev, G., Vilensky, R., Fadul, R., Redenski, I., Srouji, S., Zussman, E., 2022. Injectable Hydrogels Based on Inter-Polyelectrolyte Interactions between Hyaluronic Acid, Gelatin, and Cationic Cellulose Nanocrystals. Biomacromolecules 23, 3222-3234.
Wu, X., Guo, W., Wang, L., Xu, Y., Wang, Z., Yang, Y., Yu, L., Huang, J., Li, Y., Zhang, H., Wu, Y., Li, G., Huang, W., 2021. An Injectable Asymmetric-Adhesive Hydrogel as a GATA6+ Cavity Macrophage Trap to Prevent the Formation of Postoperative Adhesions after Minimally Invasive Surgery. Advanced Functional Materials 32, 2110066.
Xing, H., Zhang, Z., Mao, Q., Wang, C., Zhou, Y., Zhou, X., Ying, L., Xu, H., Hu, S., Zhang, N., 2021. Injectable exosome-functionalized extracellular matrix hydrogel for metabolism balance and pyroptosis regulation in intervertebral disc degeneration. Journal of nanobiotechnology 19, 264.
Xu, Y., Wushou, B., Shi, S., Liao, L., 2010. Effects of Three Anesthetic Agents in Surgery for Cricetulus migratorus and Their Selective Application. Chinese Journal of Comparative Medicine 20, 51-54.
Yang, Y., Fan, Y., Zhang, H., Zhang, Q., Zhao, Y., Xiao, Z., Liu, W., Chen, B., Gao, L., Sun, Z., Xue, X., Shu, M., Dai, J., 2021. Small molecules combined with collagen hydrogel direct neurogenesis and migration of neural stem cells after spinal cord injury. Biomaterials 269, 120479.
Zhang, G., 2018. The effects and mechanism of interferon-gamma in treating brain ischemic stroke by neural stem cells and exosomes Southeast University.
Zhang, G., Chen, L., Guo, X., Wang, H., Chen, W., Wu, G., Gu, B., Miao, W., Kong, J., Jin, X., Yi, G., You, Y., Su, X., Gu, N., 2018a. Comparative

Analysis of microRNA Expression Profiles of Exosomes Derived from Normal and Hypoxic Preconditioning Human Neural Stem Cells by Next Generation Sequencing. J Biomed Nanotechnol 14, 1075-1089.
Zhang, G., Guo, X., Chen, L., Li, B., Gu, B., Wang, H., Wu, G., Kong, J., Chen, W., Yu, Y., 2018b. Interferon-γ Promotes Neuronal Repair by Transplanted Neural Stem Cells in Ischemic Rats. Stem Cells Dev 27, 355-366.
Zhang, G., Zhu, Z., Wang, H., Yu, Y., Chen, W., Waqas, A., Wang, Y., Chen, L., 2020. Exosomes derived from human neural stem cells stimulated by interferon gamma improve therapeutic ability in ischemic stroke model. J Adv Res 24, 435-445.
Zhang, G.L., Zhu, Z.H., Wang, Y.Z., 2019. Neural stem cell transplantation therapy for brain ischemic stroke: Review and perspectives. World J Stem Cells 11, 817-830.
Zhu, Z.H., Jia, F., Ahmed, W., Zhang, G.L., Wang, H., Lin, C.Q., Chen, W.H., Chen, L.K., 2023. Neural stem cell-derived exosome as a nano-sized carrier for BDNF delivery to a rat model of ischemic stroke. Neural Regen Res 18, 404-409.

Declaration of interests

The authors declare that they have no known competing financial interests or personal relationships that could have appeared to influence the work reported in this paper.

Graphical abstract

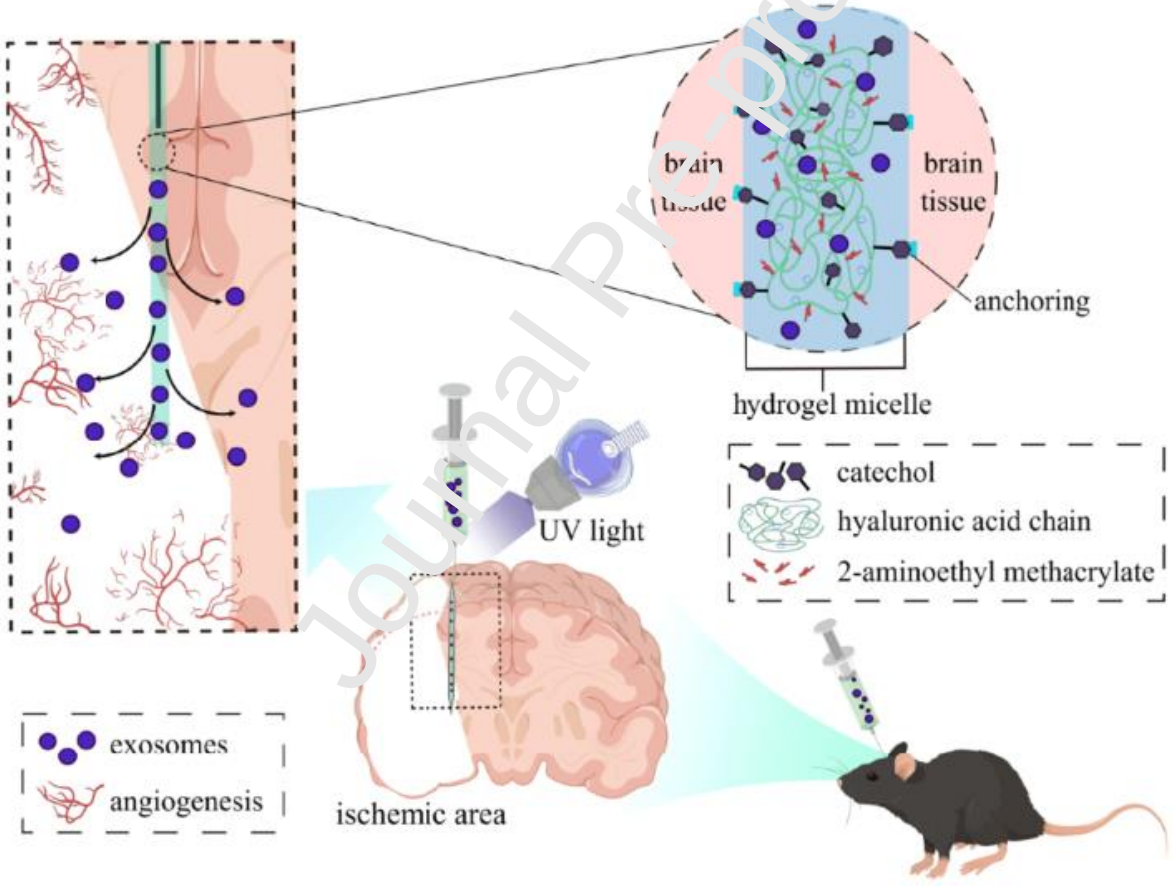

Highlights

1. The use of neural stem cells (NSCs) derived exosomes (Exos) encapsulated in a photocurable catechol-grafted hyaluronic acid (HAD) hydrogel for ischemic stroke. HAD hydrogel as a delivery scaffold is suitable for delivering and releasing exosomes continuously at the ischemic area.

2. The HAD-Exo complex maintained the biological activity of exosomes, enhanced angiogenesis and anti-inflammation at the ischemic area, and improved the cerebral infarct volume and neurological function.

3. The topically injected HAD-Exo complex provided a promising alternative strategy for clinical translation of ischemic stroke.